Budding Dynamics of Individual Domains in Multicomponent Membranes Simulated by *N*-Varied Dissipative Particle Dynamics

Bingbing Hong, Feng Qiu,* Hongdong Zhang, and Yuliang Yang

The Key Laboratory of Molecular Engineering of Polymers, Ministry of Education, Department of Macromolecular Science, Fudan University, Shanghai 200433, China

Received: September 16, 2006; In Final Form: January 26, 2007

We study the budding dynamics of individual domains in flat, multicomponent membranes using dissipative particle dynamics (DPD) simulations with varied bead number *N*, in which addition and deletion of beads based on their density at the membrane boundary is introduced. The budding process of a tubular bud, accompanied by a dynamical transition reflected in the energy and morphology evolutions, is investigated. The simulations show that budding duration is shortened with increasing line tension and depends on the domain size quadratically. At low line tension, increasing bending modulus accelerates budding at first, but suppresses the process as it increases further. In addition, the controlling role of the surface tension in the budding process is also explored. Finally, we use the *N*-varied DPD to simulate the experimentally observed multicomponent tubular vesicles, and the three bud growth modes are confirmed.

I. Introduction

Fission events occur frequently in various cellular processes, such as endo- or exocytosis, protein trafficking, and fertilization, and budding is the inevitable intermediate in the production of transport vesicles which shuttle between different cellular compartments.[1] Despite the strict modulation of lipid composition and the protein involvement in real biological membranes,[2−3] multicomponent protein-free lipid vesicles which possess intrinsic fluid characteristics and intramembrane domains are sufficient to reproduce budding and fission courses, serving as an excellent model to study the structure and function of cell membranes. In addition to the theoretical prediction that a flat domain without protein modulation can deform into a third dimension as it grows beyond a certain size,[4−8] recent experiments have also reported artificial vesicles[9−12] composed of lipids and cholesterol undergo shape transformations and topological changes similar to the in vivo observations.

Treating lipid membranes as a smooth, elastic surface with energies contributed from the membrane surface tension, the bending elasticity, and the line tension between components of lipids,[13−14] we find that many continuum models have extensively examined the equilibrium morphologies of vesicles and domains with varied compositions or under different force fields.[15−17] In a phase-separated membrane, budding or invagination are predicted as the direct results of the competition between the line tension and the membrane rigidity.[4−5,17] To investigate the dynamics of these shape transitions, several Monte Carlo (MC) simulations[6,18−19] combining dynamic triangulation were recently conducted and showed that the entire budding process can be divided into distinct time regimes. Later, Yamamoto et al.[20−21] and Laradji and Kumar[7−8] adopted a dissipative particle dynamics (DPD) method to simulate vesicular budding, taking into account the hydrodynamic interactions and area-to-volume ratio constraint. Particularly, the latter clarified the scaling laws involved in Brownian motion and the coalescence between domains or buds and related the onset time and size of domain budding to the elastic membrane properties.

However, there are still unremarked points, including (1) morphology changes from an individual domain to a bud, then to a vesicle, (2) that the smallness of the chosen system assigns considerable initial curvature to the domains before budding, whereas the domains are nearly flat on experimental giant unilamellar vesicles (GUV),[10−12] (3) that simulated surface tension increases dramatically as budding proceeds, contrary to the case of GUVs where surface tension maintains almost unvaried when a single domain bends up and buds off, and (4) relations between budding dynamics and elastic properties, especially the surface tension. A flat open membrane, mimicking a small patch from a giant vesicle, seems a plausible approach to clarify these problems. Still, the barriers are existent. They lie in the facts that the membrane patch model in canonical ensemble, where the geometry of buds are easy to measure and the elastic parameters are convenient to control, lacks the excess area necessary for budding;[7−8,18] however, on the other side, it is difficult to analyze surface tension, bud morphology, and so forth in the aggregates like vesicles, tubes, and rods where budding and fission can occur naturally. Thus, in this paper, we use the DPD method, with the hydrodynamic interactions involved, to simulate the budding process on a membrane patch, and further impose modified boundary conditions to a flat membrane patch to make the molecular number variable to deal with the abovementioned challenges.

Dissipative particle dynamics is a coarse-grained technique, first introduced by Hoogerbrugge and Koelman to describe the mesoscopic hydrodynamic behaviors of complex fluids. It is based on the interaction of soft beads, each of which corresponds to a group of several atoms. Therefore, it is able to handle much larger system sizes and time scales than atomistic simulations and, at the same time, keeps the basic chemical traits compared with continuum models. The technique is especially suitable to model equilibrium structures[22−27] and aggregation dynamics[7,8,20,21,27,28] of the systems composed of amphiphilic molecules. Many simulations of amphiphilic monolayer and bilayer

* To whom all correspondence should be addressed. E-mail: fengqiu@fudan.edu.cn.

10.1021/jp066046h CCC: $37.00
Published on Web 05/08/2007

patches have been conducted to gain insight into the molecular dependence of the elastic parameters such as bending modulus,[24,25] stretching modulus,[22] and normal and lateral stress distribution.[22,23,26] Some of the abovementioned budding and fission[21] and domain growth dynamics[7−8] have also been studied by the DPD method starting from the self-assembled fluid vesicles. Built on normal DPD, *N*-varied DPD which we introduce here is designed to simulate the open lipid membranes. We alter the boundary conditions in the simulation box through adding and deleting DPD beads according to the local density close to the boundary to make the bead number N variable. Hence, *N*-varied DPD allows the bilayer patch to stretch and contract, providing the excess area indispensable in membrane budding and fission.

The paper is organized as follows: section II presents the simulation details and the validation of *N*-varied DPD; in section III, we display the shape transform of a typical budding and fission process of an individual domain, and analyze the effects of bending modulus, surface tension, and line tension on the dynamics. As an extension of the application of *N*-varied DPD, we simulate three bud growth modes observed experimentally and discuss the stability of intermediate tubular bud thereafter. Finally, we summarize in section IV.

II. Model

A. Normal DPD. Normal DPD simulates the canonical ensemble with a constant number of beads, constant volume, and constant temperature.[29,30] Each bead in the system represents an interaction site lumped by groups of atoms. The total forces[30,31] imposing on each bead includes its direct conservative interaction with other beads $\mathbf{F}_i^{\mathrm{C}}$ and two other pairwise terms, dissipative force $\mathbf{F}_{ij}^{\mathrm{D}}$ and random force $\mathbf{F}_{ij}^{\mathrm{R}}$. The trajectory of the system is evolved by integrating Newton's laws of motion:

$$\frac{\mathrm{d}\mathbf{r}_i}{\mathrm{d}t} = \mathbf{v}_i$$

$$m_0 \frac{\mathrm{d}\mathbf{v}_i}{\mathrm{d}t} = \mathbf{F}_i^{\mathrm{C}} + \sum_{j\neq i} (\mathbf{F}_{ij}^{\mathrm{D}} + \mathbf{F}_{ij}^{\mathrm{R}}) \tag{1}$$

The vector position $\mathbf{r}_i$, the velocity $\mathbf{v}_i$, and the mass m_i define each DPD bead, with the assumption that all beads have the same mass $m_i = m_0$.

Though we modify the boundary conditions and make the bead number variable in *N*-varied DPD, the evolution law and the force field in the new model remain the same as those in normal DPD. The three kinds of forces[31] take the following form:

$$\mathbf{F}_i^{\mathrm{C}} = -\frac{\partial \Phi_i}{\partial \mathbf{r}_i} \tag{2}$$

$$\mathbf{F}_{ij}^{\mathrm{D}} = \begin{cases} -\gamma_{ij}(1 - r_{ij}/r_{\mathrm{c}})^2(\mathbf{e}_{ij}\cdot\mathbf{v}_{ij})\mathbf{e}_{ij} & r_{ij} < r_{\mathrm{c}} \\ 0 & r_{ij} \geq r_{\mathrm{c}} \end{cases} \tag{3}$$

$$\mathbf{F}_{ij}^{\mathrm{R}} = \begin{cases} \sqrt{2\gamma_{ij}k_{\mathrm{B}}T}(1 - r_{ij}/r_{\mathrm{c}})\xi_{ij}\mathrm{d}t^{-1/2}\mathbf{e}_{ij} & r_{ij} < r_{\mathrm{c}} \\ 0 & r_{ij} \geq r_{\mathrm{c}} \end{cases} \tag{4}$$

γ_{ij} is the strength of the dissipation between bead i,j and $\mathbf{v}_{ij} = \mathbf{v}_i - \mathbf{v}_j$, $r_{ij} = |\mathbf{r}_{ij}|$, $\mathbf{e}_{ij} = (\mathbf{r}_i - \mathbf{r}_j)/r_{ij}$. T represents the temperature and k_{B} is the Boltzmann constant. $\mathbf{F}_i^{\mathrm{C}}$ is expressed in the form of a gradient of the potentials Φ_i involving bead i. Both $\mathbf{F}_{ij}^{\mathrm{D}}$ and $\mathbf{F}_{ij}^{\mathrm{R}}$ are limited to a range r_{c}. By keeping the mean diffusion as a constant, for example, independent of the time step of the integration, Groot and Warren[31] derived the factor $\mathrm{d}t^{-1/2}$ in eq 4. The randomness of $\mathbf{F}_{ij}^{\mathrm{R}}$ is contained in the uniform random variable $\xi_{ij}(t)$, which generates elements that are independent for each pair of beads and for each time step, and has zero mean and unit standard deviation:

$$\overline{\xi_{ij}(t)} = 0 \qquad \overline{\xi_{ij}(t)\xi_{kl}(t')} = \delta(t - t')(\delta_{ik}\delta_{jl} + \delta_{il}\delta_{jk}) \tag{5}$$

In the previous simulations of the lipid membrane,[22−26] three types of potentials φ_1, φ_2, and φ_3, all of which are components of Φ_i, are conventionally chosen to model the conservative interactions of bead i with its neighbors. Nonbonded beads repel softly against each other with the soft repulsion potential φ_1-(i,j) cut off at the distance r_c:

$$\varphi_1(i,j) = \begin{cases} \frac{1}{2}a_{ij}\left(1 - \frac{r_{ij}}{r_{\mathrm{c}}}\right)^2 & r_{ij} < r_{\mathrm{c}} \\ 0 & r_{ij} \geq r_{\mathrm{c}} \end{cases} \tag{6}$$

where a_{ij} is the maximum repulsion between beads i and j. Beads within the same lipid are connected together through harmonic spring potentials:

$$\varphi_2(i,i+1) = \frac{1}{2}k_{\mathrm{b}}(r_{\mathrm{b}} - r_{i,i+1})^2 \tag{7}$$

where k_{b} is the spring coefficient and r_{b} is the equilibrium bond length. For semiflexible surfactants or lipids with more than one tail, additional three-body chain stiffness potentials are needed to help construct the complicated molecular architectures:

$$\varphi_3(i-1,i,i+1) = k_{\mathrm{c}}[1 - \cos(\theta_i - \theta_i^{\mathrm{sp}})] \tag{8}$$

where k_{c} is the chain modulus, and the angle θ_i is defined by the scalar product of the two vectors pointing from $i-1$ to i and from i to $i+1$, respectively. The spontaneous angle θ_i^{sp} are usuallly set to zero for the linear lipids but occasionally are set to a finite value to build a triple with a preferred tilt angle.

In our model, one water bead stands for approximately three water molecules, and a simple surfactant architecture of HT_3 is considered to model the lipid, where H and T stand for the hydrophilic head bead and hydrophobic tail bead, respectively. Although many previous researches have investigated the static properties of the bilayer membrane composed of the lipids with longer chains or more than one tail, few DPD simulations have ever employed these complex molecules to study the dynamic behaviors of the lipid aggregates because of the heavy computational load involved in diminishing the effect of the membrane thickness for longer molecules. Thus, our simulation is conducted on as simple molecular architecture as possible.

We set the parameters in the conservative force as follows:

$$a_{ij} = \frac{k_{\mathrm{B}}T}{r_{\mathrm{c}}}\begin{pmatrix} & \mathrm{W} & \mathrm{H_A} & \mathrm{T_A} & \mathrm{H_B} & \mathrm{T_B} \\ \mathrm{W} & 25 & 25 & 75 & 25 & 75 \\ \mathrm{H_A} & 25 & 25 & 75 & a & 75 \\ \mathrm{T_A} & 75 & 75 & 25 & 75 & a \\ \mathrm{H_B} & 25 & a & 75 & 25 & 75 \\ \mathrm{T_B} & 75 & 75 & a & 75 & 25 \end{pmatrix} \tag{9}$$

where W, H, and T represent the water bead, the head bead and the tail bead, respectively, and the subscripts A and B stand for two kinds of lipids. We vary the parameter a in eq 9 to model the role played by the interfacial line tension between lipid components A and B. It is necessary to point out that the

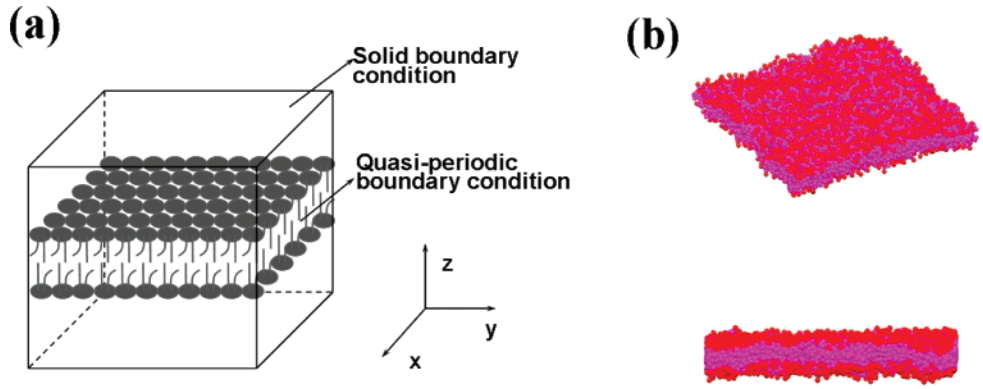

Figure 1. Single-component membrane patches in *N*-varied DPD. (a) Boundary conditions in *N*-varied DPD in which the bilayer membrane is arranged perpendicular to the *z* axis. "Quasi-periodic boundary condition", which combines both the standard periodic boundary condition and the addition and deletion of beads, is imposed on the box sides perpendicular to the membrane plane; "solid boundary condition" includes two $2r_c$-thick layers of immobile water beads and specular reflection for beads that cross the wall positions. (b) Snapshots of a bilayer membrane patch composed of 2492 lipids in a $32 \times 32 \times 36r_c^3$ simulation box, where UCDL = 2.19 lipids/r_c^2, LCDL = 0.44 lipids/r_c^2, and $k_c = 3.0k_BT$.

relation of $a_{WH} > a_{HH}$ in some early studies[22,23] of the membrane equilibrium structures would easily lead to unphysical phenomena like crinkling, clustering of lipid heads, burial of the head clusters into the membrane bulk, and so forth when the membrane transforms significantly, since these behaviors substitute the less repulsive H-H pairs for stronger W-H ones and reduces the total energy. Thus, a_{WH} and a_{HH} are fixed at the same value in our simulation.

The dissipation strength γ_{ij} is set at $\gamma_{ij} = 20[(k_BT)m_0/r_c^2]^{1/2}$ for hydrophobic interactions (water-tail, head-tail) and $4.5[(k_BT)m_0/r_c^2]^{1/2}$ for others.[22−23] The introduction of different γ_{ij} values helps to enhance the efficiency of the thermostat in a system where the presence of chain stiffness potential (eq 8) intensifies the bead collision and consequently raises the temperature. The spring and the chain stiffness parameters have the values $k_b = 128k_BT/r_c^2$, $r_b = 0.5r_c$, and $\theta_i^{sp} = 0$. Similar to *a* in eq 9, different k_c's are chosen for lipids with different chain moduli, which result in different membrane bending moduli κ. The values of m_0, r_c, and k_BT are assigned as unit.

Finally, The equations of motion are integrated by a self-consistent leapfrog scheme proposed by Pagonabarraga et al.,[32] with a time step Δt equal to $0.05[m_0r_c^2/(k_BT)]^{1/2}$. The scheme is reported to display better time reversibility and temperature-conserving efficiency than the widely used VV-style algorithms.[33]

B. *N*-Varied DPD. Two kinds of tensions are present in our simulation. One is called surface tension, measuring the stress anisotropy induced by the membrane−water interactions.[22,34] The other tension rises from the incompatibility between the coexisting lipid components and exists around the domain which consists of lipids that differ from those composing the mother membrane. We denote it as line tension hereafter.

In normal DPD, the conservation of lipid number in the membrane will bring in increasing surface tension when the flat membrane patch bends up. So, unlike the case of some closed aggregates whose large area-to-volume ratio offers sufficient excess area to release the tension, large deformations, for example, budding and fission, are prohibited in the *N*-invariant simulation of the flat membrane patches. There are two other candidate techniques probably available for the excess area supplement. One is a constant surface tension simulation[24] in which the system remains to be NVT (canonical) ensemble. However, the membrane bumps up and even experiences topological changes as budding proceeds. Hence, calculation of the surface tension using the Kirkwood equation[34] which is specially designed for a flat surface in a bead-based system becomes invalid. No implementable method has ever been derived to determine the surface tension of a curved surface consist of interacting beads. The other technique is to make the simulation box an open system to the matter exchange with its environment. It is believed that living cells keep lipid reservoirs at a fixed chemical potential to maintain the surface tension of most of their membranes at a constant level.[1] Thus, an application of a grand canonical ensemble seems to be a natural solution. In practice, however, the heterogeneous boundary and the dynamic nature make the calculation of the instant chemical potential profiles rather time-consuming and statistically not precise.

Therefore, instead of the chemical potential criteria, we propose the density criteria by which the entering or leaving of a molecule is determined. In essence, new lipid molecules are added to a boundary position where the local density of the membrane is less than a predefined bottom value, and a few lipid molecules should be deleted when the local boundary density exceeds the upper ceiling. The treatment for water is similar. Since the chemical potential is a monotonic function of density, it is actually an indirect but convenient approach to maintain the local boundary chemical potential fixed. Figure 1a shows the boundary conditions in *N*-varied DPD.

Note that we put the prefix "quasi-" before the phrase "periodic boundary condition" for the box sides perpendicular to the membrane plane. The condition resembles the standard periodic boundary conditions,[35] on the one hand, in that if a bead leaves the box then it should be replaced by an image bead that enters from the opposite side. On the other hand, it differs from the latter whenever a sparsely populated region appears in the vicinity of the membrane boundary, then additional lipid molecules are inserted. Similarly, whenever a densely populated region occurs near the membrane boundary, lipid molecules are deleted. The condition for water beads is similar. For the box sides parallel with the membrane plane, we place a $2r_c$-thick layer of immobile water beads to model the solid boundary conditions. The solid walls ensure the pressures exerted on both the membrane sides to be transferred only through the bilayer. We further impose reflection of the beads at the solid boundary:[35]

$$\begin{aligned} &\text{if } z_i(t+\Delta t) < 0 \quad \text{then } z_i(t+\Delta t) = -z_i(t+\Delta t), \\ &\qquad\qquad v_{i,z}(t+\Delta t) = -v_{i,z}(t+\Delta t) \\ &\text{if } z_i(t+\Delta t) > L_z \quad \text{then } z_i(t+\Delta t) = 2L_z - z_i(t+\Delta t), \\ &\qquad\qquad v_{i,z}(t+\Delta t) = -v_{i,z}(t+\Delta t) \end{aligned} \quad (10)$$

TABLE 1: Determination of Surface Tension on the Final Mophologies of Individual Domains ($k_{cA} = 3.0k_BT$)

interface tension (k_BT/r_c^2)	line tension parameter (a)	bending rigidity: $k_{cA}/k_{cB} = 3.0/0.0$, $\kappa_A/\kappa_B = 2.34 \pm 0.27k_BT/1.67 \pm 0.22k_BT$	bending rigidity: $k_{cA}/k_{cB} = 3.0/1.5$, $\kappa_A/\kappa_B = 2.34 \pm 0.27k_BT/1.98 \pm 0.24k_BT$
0.82 ± 0.06 UCDL/LCDL = 1.87/0.50	50.0	rupture	rupture
	40.0	rupture	flat B phase
0.055 ± 0.018 UCDL/LCDL = 2.19/0.44	50.0	rupture	curved B phase
	40.0	curved B phase	curved B phase
-0.23 ± 0.05 UCDL/LCDL = 2.13/0.50	50.0	budding, pinched off by cleavage	budding, pinched off by cleavage
	40.0	budding, pinched off through hemifission intermediate	budding, pinched off through hemifission intermediate

TABLE 2: Determination of Surface Tension on the Final Mophologies of Individual Domains ($k_{cA} = 0.0k_BT$)

interface tension (k_BT/r_c^2)	line tension parameter (a)	bending rigidity: $k_{cA}/k_{cB} = 0.0/0.0$, $\kappa_A/\kappa_B = 1.67 \pm 0.22k_BT/1.67 \pm 0.22k_BT$	bending rigidity: $k_{cA}/k_{cB} = 0.0/1.5$, $\kappa_A/\kappa_B = 1.67 \pm 0.22k_BT/1.98 \pm 0.24k_BT$
0.91 ± 0.05 UCDL/LCDL=1.87/0.37	50.0	rupture	rupture
	40.0	rupture	rupture
0.33 ± 0.03 UCDL/LCDL=2.00/0.37	50.0	curved B phase	rupture
	40.0	curved B phase	flat B phase
-0.013 ± 0.008 UCDL/LCDL=1.87/0.50	50.0	budding, pinched off by cleavage	budding, pinched off by cleavage
	40.0	budding, pinched off through hemifission intermediate	budding, pinched off through hemifission intermediate

z_i and $v_{i,z}$ are the z components of the position and the velocity of bead i, respectively. L_z stands for the box dimension in the z direction (not including the two $2r_c$-thick layers of frozen water).

In implementation of the density criteria, the water phase and the lipid phase are dealt with separately. We get the local water density of an r_c^3-volumed cubic by averaging the total number of water beads in its neighboring region over the region volume $27r_c^3$. As for the lipid phase which takes on an almost flat fluid membrane around the box sides, the area density calculated within an r_c^2-sized projected area is adopted instead. Because of the region size selected above, addition or deletion of one water bead or one whole lipid molecule in the specific region each time step is enough to drive the local density back into a defined value. The momentum of a newly added bead is assigned from a Gaussian distribution with zero mean and $(k_BT)^{1/2}$ variance.

The upper critical density of water (UCDW) above which a water bead should be deleted from the box is set $3.5r_c^{-3}$, and the lower critical density of water (LCDW) below which an addition operation is needed equals $2.5r_c^{-3}$. The chosen UCDW and LCDW ensure the average density for a pure water system be brought along to a fluctuating value that is not far deviated from $3.0r_c^{-3}$, no matter whether the system is initialized with overflowing water beads or deficient. On the other end, they are not so close to each other to raise the temperature by the frequent adding and deleting operations. The system temperature fluctuates within 1%, as conserved as that of normal DPD. As for the lipid phase, we find the upper and lower critical densities of lipids (UCDL and LCDL, respectively) directly set the average projected area per lipid throughout the membrane, therefore tightly related to the surface tension, which means the statistical ensemble of N-varied DPD is a variant of μVT ensemble (or correspondingly, constant surface tension ensemble). In fact, the upper critical density (UCD) and lower critical density (LCD) uniquely define an average density of each phase, which further sets a fixed chemical potential for both lipids and water, or a fixed surface tension for the membrane. Different surface tensions in N-varied DPD are then realized by applying different sets of UCD and LCD, and their influence on the budding dynamics will be discussed in section IIIC.

In our simulation, the elastic properties are computed in a $32 \times 32 \times 36r_c^3$ box (including two $2r_c$-thick layers of wall) with an equilibrated single-component bilayer, while the budding and fission courses take place in a $50 \times 50 \times 74r_c^3$ box (including walls) wherein the boundary effects on the large shape deformation are diminished. Previous researches have reported all of the details of calculating the properties of the elastic membranes, for example, surface tension,[36−37] bending modulus,[24−25] diffusion coefficient,[36] and so forth. Here, we only give a brief description of the calculation procedure.

The surface tension σ of a bilayer is directly related to the three diagonal components P_{xx}, P_{yy}, and P_{zz} of the z-dependent local pressure tensor $\mathbf{P}(z)$ by

$$\sigma = \int_0^{L_z} \left[P_{zz}(z) - \frac{1}{2}\left(P_{xx}(z) + P_{yy}(z)\right) \right] \mathrm{d}z \qquad (11)$$

where the integration is taken over the whole system except the two $2r_c$-thick layers of frozen water. To determine the pressure tensor profile along the z axis, we partition the simulation box into layers (denoted by $L(z)$) parallel to the membrane and of equal thickness $\Delta z = r_c/8$. The z coordinate of layer $L(z)$ begins from z and ends at $z + \Delta z$. Then the local pressure tensor is given as

$$\mathbf{P}(z) = \sum_{i \in L(z)} m_i \mathbf{v}_i \otimes \mathbf{v}_i - \sum_n \left[\frac{1}{nL_xL_y\Delta z} \sum_j \sum_{(k,l)} (\nabla_{j_k}\varphi^{(n)} - \nabla_{j_l}\varphi^{(n)}) \otimes \mathbf{r}_{j_k j_l} f(z_{j_k}, z_{j_l}, z) \right] \qquad (12)$$

The first term is the kinetic contribution from all of the particles lying in layer $L(z)$. In the second term, L_x and L_y are the system

box dimensions along x and y directions, respectively. $\varphi^{(n)}$ denotes n-body potential. The summation over j includes all of the interactions involving n beads, and (k,l) means summing over all possible bead pairs in the n-body interaction j. The weight function $f(z_1, z_2, z)$ is defined by

$$f(z_1, z_2, z) \equiv \begin{Bmatrix} \theta(z_1 - z)\theta(z + \Delta z - z_1) & \text{for } z_1 = z_2 \\ \dfrac{1}{z_2 - z_1}\displaystyle\int_{z_1}^{z_2} \theta(z' - z)\theta(z + \Delta z - z')\mathrm{d}z' & \text{for } z_1 \neq z_2 \end{Bmatrix} \quad (13)$$

where θ is the Heaviside function with $\theta(z) = 0$ for $z < 0$, $\theta(z) = 1$ for $z > 0$, and $\theta(z) = 1/2$. The weight function $f(z_1, z_2, z)$ serves to distribute the summand in the second term of eq 12 averagely among the layers between j_k and j_l.

The chain modulus k_c reflects the bending rigidity of membranes. Lipids with larger k_c constitute a more rigid membrane. So, we use k_c to indicate the membrane rigidity in most parts of the paper. In Tables 1 and 2, we only present several bending moduli κ, and they are estimated by the simple relation $\kappa = Kl^2/48$, where l is the membrane thickness, and the stretching modulus of the membrane K is defined as

$$\sigma = K\left(\frac{A - A_0}{A_0}\right)$$

Here, A is the projected area per lipid, and A_0 is the projected area of a lipid when the surface tension is zero. The linear relation holds only when A is close to A_0.

The lateral diffusion coefficients of lipids in the membrane are calculated in NVT ensemble, because the addition and deletion operations in N-varied DPD may unphysically disturb the diffusion behaviors of the lipids which cross the boundary.

$$D_L = \lim_{t\to\infty} \frac{\sum_i [\mathbf{r}_{||}(t) - \mathbf{r}(0)]^2}{4N_L t} \quad (14)$$

Equation 14 shows how to calculate the lateral diffusion coefficient of lipids D_L. The variable $\mathbf{r}_{||}(t)$ is the lateral component of the lipid position $\mathbf{r}(t)$, and N_L is the lipid number in the membrane.

C. Validation. Figure 1b shows a snapshot of an equilibrated membrane patch composed of HT_3 with $k_c = 3.0k_BT$ and lipid density criteria UCDL = 2.19 lipids/r_c^2 and LCDL = 0.44 lipids/r_c^2 (UCDL and LCDL are area density values in one monolayer), in a $32 \times 32 \times 36r_c^3$ box. The average equilibrium number of lipid molecules is then set to be 2510.5, and surface tension $\sigma = (0.055 \pm 0.018)k_BT/r_c^2$. The instant lipid number is 2492 in the snapshot. We present in Figure 2 the time evolutions of bead numbers of each component in systems with the same force field parameters and boundary conditions as those in Figure 1b. It shows that the fluctuating range of the equilibrium water-bead number in a system initially filled with dense water phase overlaps with that of a sparsely filled system. Similarly, the number of lipid molecules drops sharply to the equilibrium range if the initial value is overestimated but rises in the same manner in the case of low value at the beginning. The two insets give an enlarged view of the bead number evolutions before equilibrium and show that the final deviations of water and lipid molecules from their equilibrium values are less than 0.25% and 2%, respectively.

Each set of UCDL and LCDL defines an equilibrium lipid density in the membrane, which further determines the surface tension. To choose a set of UCDL/LCDL for the bud formation, one must ensure that the equilibrium surface tension under the chosen UCDL/LCDL is close to zero, a condition that budding could take place (less than 0.01 mN/m^2).[17] In addition, UCDL and LCDL should not be chosen to be too far apart. The membrane needs to relax to an equilibrium state quickly. On the other end, one has to make the two values not so close to each other as to raise the temperature by the frequent adding and deleting operations. Although the UCDL and LCDL differ by a factor 5, this only occurs at a narrow boundary, which is a small portion of the membrane. Also, the molecular density of the main body of the membrane keeps constant in the simulation, which means the compressibility of the membrane is rather small.

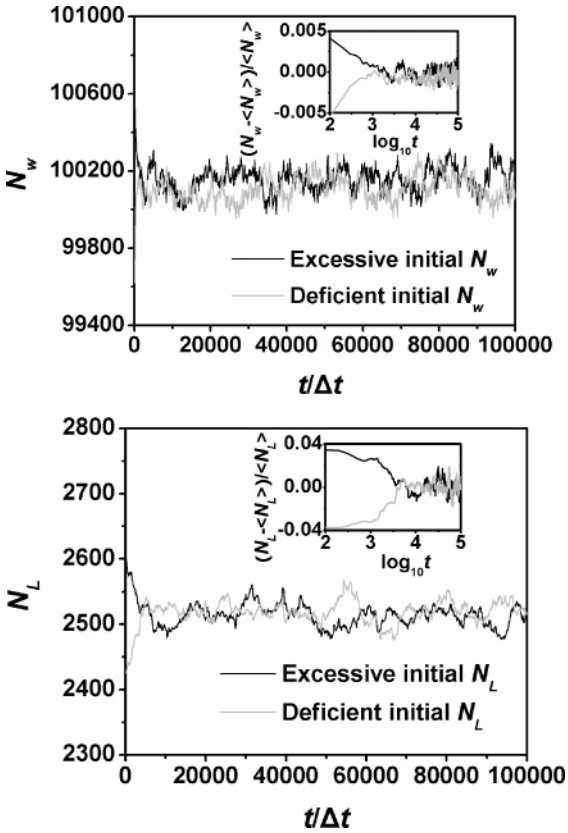

Figure 2. Evolutions of the numbers of water beads (N_W) and lipid molecules (N_L). The two insets enlarge the number evolutions before equilibrium and show the deviations of instant water and lipid molecules from their equilibrium values.

Figure 3 indicates the fluctuations of the total momenta along the three axes. The exchange of beads with the environment intensifies the noise of momentum fluctuation in each direction but does not result in cumulative deviation from zero. The fluctuations of x and y momenta reveal the overall motion of the whole system. Because of the quasi-periodic boundary conditions, the centers of mass of lipids and water beads drift randomly in the directions parallel to the membrane. In contrast, the overall motion along the z axis is limited by the solid boundary conditions, leading to a frequently vibrating momentum.

D. Initial Conditions for Budding and Fission. After a single-component (labeled as A) membrane equilibrates under the given boundary conditions, the budding and fission process is initialized by relabeling the lipids within a circular domain as a B component. Although the scattered lipids are observed to aggregate into floating domains if the B component is relabeled randomly, we do not use this strategy for domain

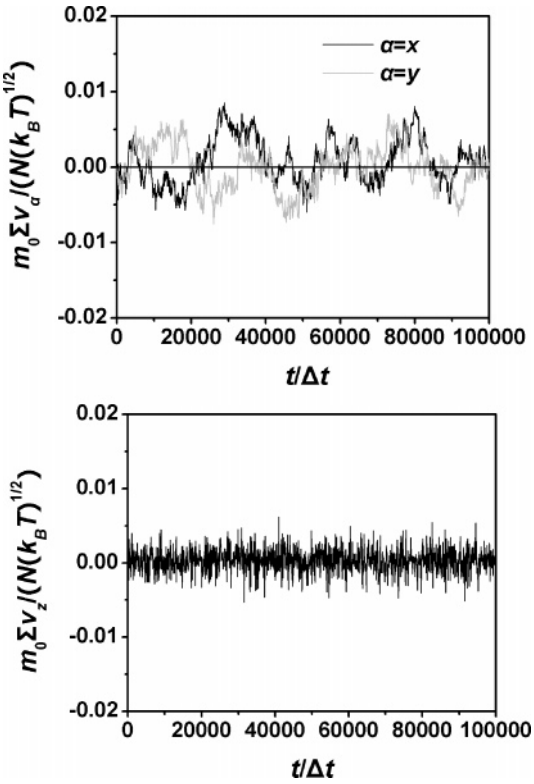

Figure 3. Fluctuations of total momenta along the *x*, *y*, and *z* axes. *N* is the instant total number of beads in the system, and $(k_BT)^{1/2}$ is the average velocity along any axis.

formation because domains may drift across the boundary where the addition and deletion operations may cause unexpected results. All of the parameters for component A remain the same before and after relabeling. The radius of the domain labeled in the upper leaflet is $1r_c$ larger than that of the domain labeled in the lower leaflet, which creates the initial perturbation that promotes the lipids of B component moving toward the upper membrane side with the larger domain. This strategy is necessary especially for large domains, where the membrane undulations would significantly reduce the chance of the overall one-sided departure of B domain from the membrane plane. Thus, constriction of the interface between component A and component B will lead to wrinkling of the domain, instead of budding, if the domain sizes within the two leaflets are initialized equally. Normally, great computational costs are required in such a case before the domain evolves into a configuration which favors one-sided bending over wrinkling. So the $1r_c$ difference in radius is a trick to reduce the computer load and serves to facilitate the onset of the budding process.

III. Results and Discussion

A. Budding and Fission of a Single Domain. Figure 4 shows a typical process of budding from a flat, circular domain and subsequent fission into a vesicle in a $50 \times 50 \times 74r_c^3$ box. The parameter a is set to be 40.0 in eq 9. The boundary condition UCDL/LCDL = $2.13r_c^{-2}/0.50r_c^{-2}$ with chain modulus $k_{cA} = 3.0k_BT$ determines the surface tension $\sigma = (-0.23 \pm 0.05)k_BT/r_c^2$ for a single-component membrane. The surface tension here is slightly negative, but still close to zero, and we will discuss it further in section IIIC. Initial domains composed of component B with $k_{cB} = 3.0k_BT$ are labeled $11.5r_c$ for the upper monolayer and $10.5r_c$ lower in radius (Figure 4a,a′), which creates a perturbed upward translation of the entire domain. As the line

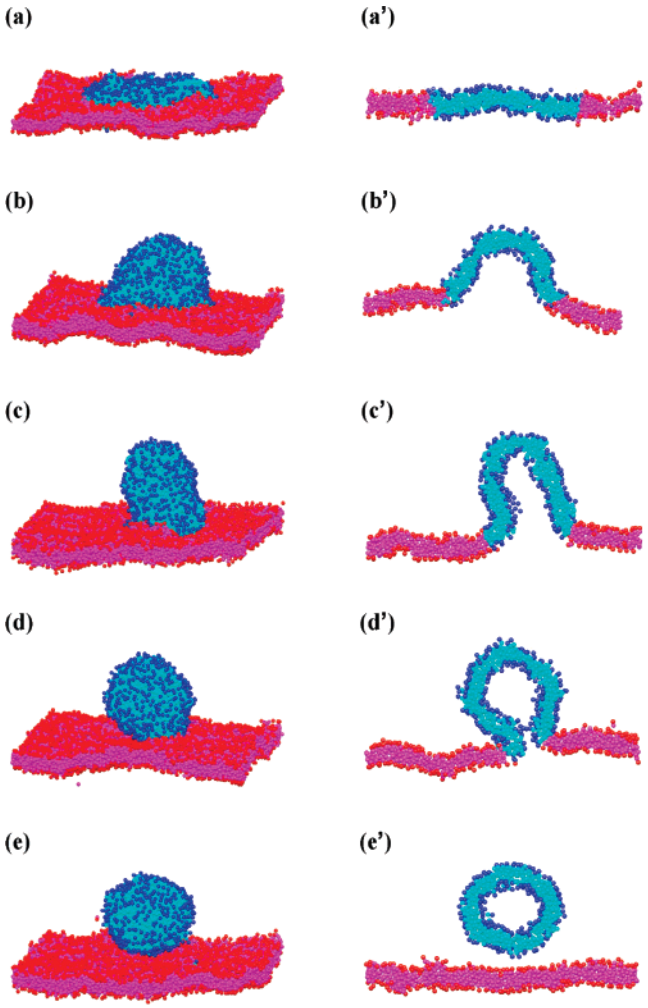

Figure 4. Snapshots of budding and fission of a single domain with t = (a) $0\Delta t$, the flat domain (b) $11\,500\Delta t$, the cap (c) $26\,000\Delta t$, the tubular bud (d) $34\,000\Delta t$, the bud with a constricted neck, and (e) $40\,000\Delta t$, the vesicle and (a′)−(e′) their corresponding sliced images.

tension drives the constriction of the interfacial length around the domain edge, the domain bends up into a cap-shaped bud (Figure 4b,b′) and further a tubular bud (Figure 4c,c′). The budding process then continues with the formation of a constricted neck (Figure 4d,d′) and finally ends with the severing of the neck and the separation of a vesicle from the mother membrane (Figure 4e,e′). The whole process can be divided into five stages corresponding to the bud morphologies in the five snapshots in Figure 4, namely, the flat domain, the cap-shaped bud, the tubular bud, the bud with a constricted neck, and the vesicle. Here, the formation of a tubular bud is a particular phenomenon that is absent from the continuum theories. It probably arises from the effect of membrane thickness. Experiments of budding dynamics on a multi-lamellar tube where the area-to-volume limit is eliminated also confirm the existence of a tubular bud intermediate.[12] The tubular bud in Figure 4 lasts approximately $5000\Delta t$. We will discuss in section IIID that, when supplemental lipids of B component float around the object domain, the bud grows longer and its life span is elongated.

All of the energy changes pertinent to the B component are calculated from the conservative interactions and are presented in Figure 5. As the domain deforms out of the membrane plane, the interfacial energy arising from the line tension around the

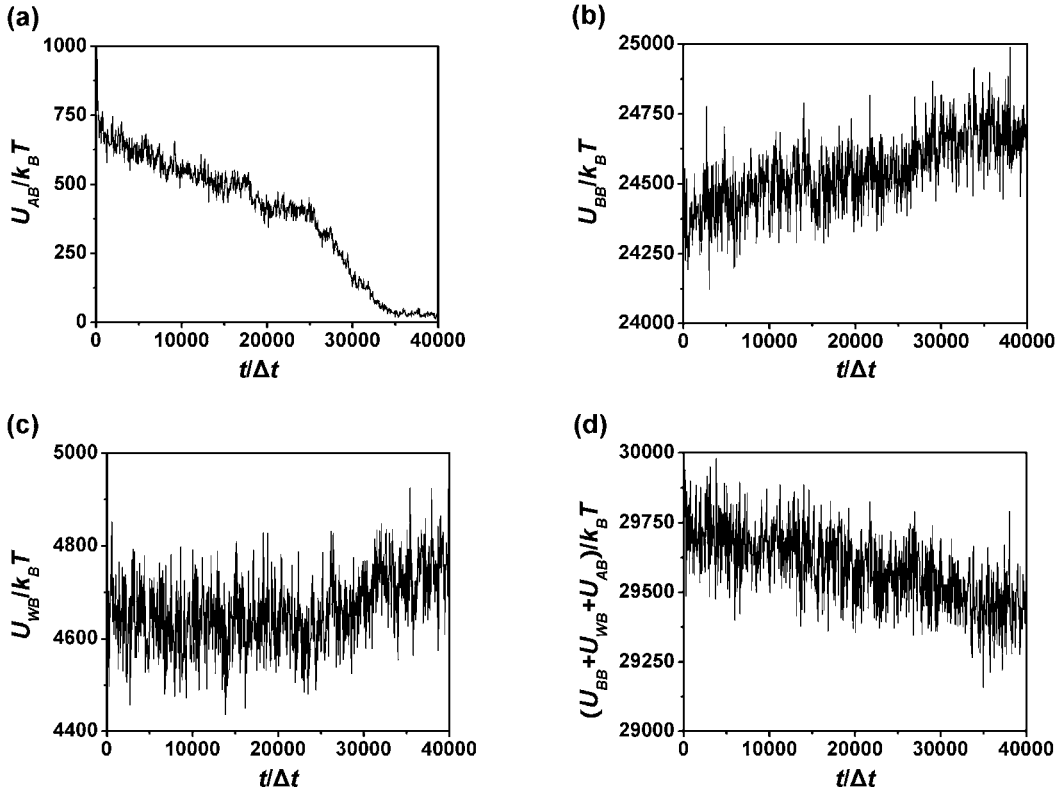

Figure 5. Evolutions of (a) interface energy originating from the line tension between the two lipid components, (b) energy within the domain bulk, a measure of the bending energy, (c) domain−water surface energy, and (d) total energy of B domain, equal to the summation of the energies in (a)−(c).

domain decreases until the bud is pinched off, which occurs after around 33 000Δ*t* (Figure 5a). The nonzero residue value of the interfacial energy after vesiculation is attributed to the interactions between A lipids and several remaining individual B lipids that have detached from the domain and are left in the mother membrane. Figure 5b shows a rise of the bulk energy, which only includes B−B interactions. To some extent, it is a measure of the domain's bending energy. The monotonic increase of the bulk energy over increasing mean curvature throughout the budding process suggests that the spontaneous curvature introduced by the unequal domain sizes in the two leaflets is not significant. In Figure 5c, the surface energy rising from the domain−water interactions remains constant at the early time but, beyond our expectation, begins to increase after about 26 000Δ*t*. We will discuss the transition below. The total domain energy in Figure 5d which is the summation of the three kinds of energy in Figure 5a−c falls steadily. It demonstrates the competition between the interfacial energy and the bending energy during the budding process, as predicted in the elastic theory of membrane.[4,5,17] In the budding case discussed here, the decrease in the interfacial energy between component A and component B exceeds the gain in the bending energy and the domain−water surface energy and behaves as the driving force inducing the budding process.

Both Figure 5a and Figure 5c exhibit a clear transition around 25 000Δ*t*. Inspection of the budding process shows that a tubular bud with approximately equal radii on the top and at the root (Figure 4c,c′) forms around the transition point. This is not coincident. We will show here that the formation of a tubular bud is responsible for the transition in Figure 5a, and we will show in the next paragraph that the tubular configuration also determines the transition in Figure 5c. In Figure 5a, the interfacial energy, which is proportional to the interfacial length between the lipid components, A and B, decreases slowly with time in a roughly linear manner before the formation of a tubular bud. However, after the transition point, it falls with a larger slope, indicating that an additional barrier is present in the early stage of budding. The time evolutions of the bud morphology in Figure 6 show the bud reaches its tallest configuration at the transition point. Thus, we infer the obstruction stems from the hydrodynamic drag force. The hydrodynamic drag force is an energy-dissipating force only exerted on a moving or deforming object in fluids and originates from the friction between the object and the fluid, the local relative velocity and the pressure of the fluid around the object.[38] As the bud rises from a flat domain to an upright configuration, it has to push away the water above it and near its root and therefore bears the relative velocities to the water both at the top and at the root. So the hydrodynamic drag forces f_{D1} and f_{D2} (Figure 7) in the horizontal and vertical directions, respectively, exert on the domain until the bud grows to the tallest shape at the transition point. In the succeeding deformations, only the constriction of the neck continues, but the bud no longer grows taller. So, f_{D2} disappears, and f_{D1} is limited to the neck region, leading to the acceleration of constriction of the domain edge in the late budding stage.

As for Figure 5c, we make a crude estimation to explain the transition in the domain−water surface energy (proportional to the surface area) by assuming that the bud is a part of a perfect spherical surface and that a plane $x_1 d$ distant from the inner surface conserves the area density during the budding process, with $0 < x_1 < 1$ and d the bilayer thickness (Figure 8a). So the area of the plane keeps constant throughout.

$$2\pi rh = \pi R_0^2 \tag{15}$$

R_0 denotes the initial radius of the plane when it is flat, r is the instant radius of the spherical surface where the constant-area

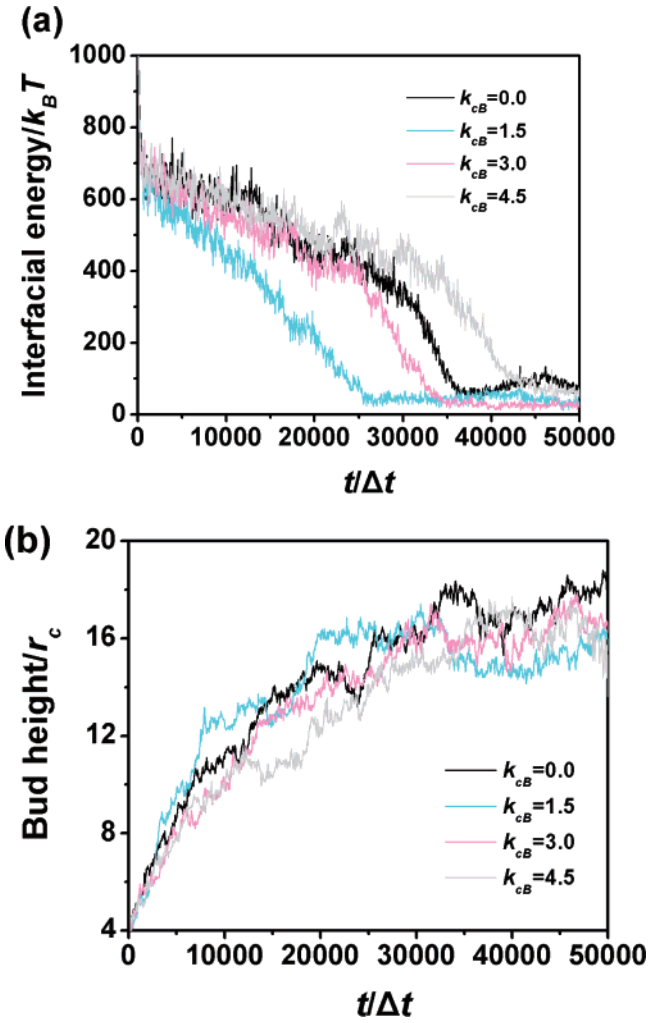

Figure 6. Evolution of bud morphologies from the domains with different bending moduli (a = 40.0). The chain modulus of lipid component B, k_{cB}, is used to measure the bending modulus κ. A larger chain modulus indicates a harder membrane. (a) Evolution of the interfacial energy, which is proportional to the interfacial length between lipid components A and B. (b) Evolution of bud height, indicating that the buds reach the tallest configuration at the transition point of their corresponding interfacial energy curves in (a).

plane lies during budding, and h is the height of the curved plane. The domain−water surface area S can then be estimated as

$$S = S_{in} + S_{out} \approx 2\pi(r - x_1 d)(h - x_1 d) + 2\pi(r + (1 - x_1)d)(h + (1 - x_1)d)$$
$$= S_0 + 2\pi(1 - 2x_1)d\left(r + \frac{R_0^2}{r}\right) \quad (16)$$

where S_0 is constant and equal to $2\pi R_0^2 + 2\pi x_1^2 d^2 + 2\pi(1 - x_1)^2 d^2$. This equation reflects the dependence of the domain−water surface area on the bud curvature ($1/r$). Since the lipid densification causes the rise of the pairwise interactions, it is valid to further limit x_1 to the range $0 \sim 1/2$. Figure 8b shows the dependence indicated by eq 16. The surface area decreases gently as the domain curves up, until a hemispherical configuration is formed with $r = \sqrt{2}R_0/2$. Afterward, we observe a sharp increase in the surface area when the domain edge continues to constrict. However, the assumed constant-area plane is rarely present in simulation. Actually, x_1 fluctuates, and the bud hardly keeps in the spherical surface. So the gentle decline before the transition is concealed in Figure 5c by the large fluctuations when the bud curvature is small, but the rising tendency is still observable at the late budding stage when the bud curves highly.

B. Effects of Line Tension, Bending Modulus, and Domain Size. We examine the roles of line tension and bending modulus in the budding process. The results in Figure 9 are obtained from a series of simulations of two-component membranes with varied line tension parameter a and $k_{cA} = k_{cB} = 3.0k_BT$. We use the period from the beginning to the point when the interfacial length drops to zero as a measure of the lifetime of a bud or budding duration. Within our expectation of the budding induced by the intramembrane domain,[4,5] the increasing line tension shortens the budding duration effectively. The transitions in the interfacial length between lipid components, A and B, are also observed in Figure 9a, except the curves with considerably high line tensions a = 60.0 and 65.0, where the effects of the hydrodynamic drag become negligible. Combining both Figure 9a and Figure 9b, we gain the same observation as in Figure 6 that the bud evolves to the tallest shape when the transition occurs, and afterward, the interface begins to constrict faster.

Figure 10 illustrates the influences of the line tension and bending modulus on the budding dynamics in systems with $k_{cA} = 3.0k_BT$ and varied k_{cB}. Note that here the bending modulus of the membrane is characterized by the chain modulus, since the lipids with larger chain modulus constitute a harder membrane. The budding durations of all domains decline significantly over the increasing line tension. However, the case becomes more complicated for the role of bending modulus. In the low line tension range, the budding process is shortened as k_{cB} increases from 0 to $1.5k_BT$ (Figure 6a), but when the chain modulus of lipid B rises from $1.5k_BT$ to $4.5k_BT$, budding is almost slowed by one time (Figure 10). In contrast, in the case of high line tension, the budding process is not significantly affected by the bending modulus. Here, we believe that the bending modulus actually incorporates several factors which may affect budding. For a very soft membrane, the relatively large thermal fluctuations prevent the disturbance induced by the driving force at the domain boundary from transferring effectively to the central domain region, so the budding process is considerably delayed. However, if the bending modulus becomes larger than a certain value above which the thermal fluctuations are not important, then the whole process is elongated due to the raised dominance of bending energy.

We present the effects of the initial domain size R_0 on budding dynamics in Figure 11, obtained from the systems where UCDL/LCDL = $2.13r_c^{-2}/0.50r_c^{-2}$ and $k_{cA} = k_{cB} = 3.0k_BT$. The simulations on both low and high line tensions reveal a quadratic domain-size dependence of budding duration. The results agree with the fluid character of the lipid membrane and satisfy eq 17 if we ignore the interactions between domains or between individual lipids and the domain.

$$t \sim \frac{R_0^2}{D_L} \quad (17)$$

D_L stands for the lateral diffusion constant of individual lipids.

C. Surface-Tension Controlled Budding. We have mentioned in section II that the surface tension of the membrane is related to the UCDL and LCDL which control the average projected area per lipid. In previous simulations, UCDL/LCDL = $2.13r_c^{-2}/0.50r_c^{-2}$ and $k_{cA} = 3.0k_BT$ are adopted, defining a surface tension around $-0.23k_BT/r_c^2$. The minus indicates the

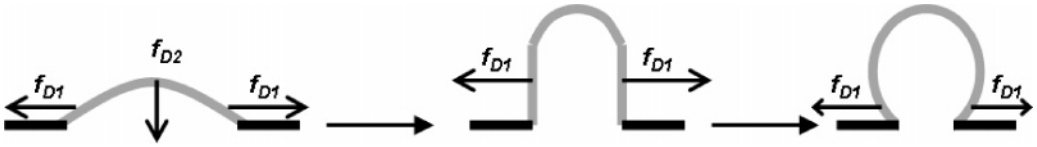

Figure 7. Schematic representations of the hydrodynamic drag forces f_{D1} and f_{D2} exerted on the bud. The A phase is colored by black, and the B phase is gray.

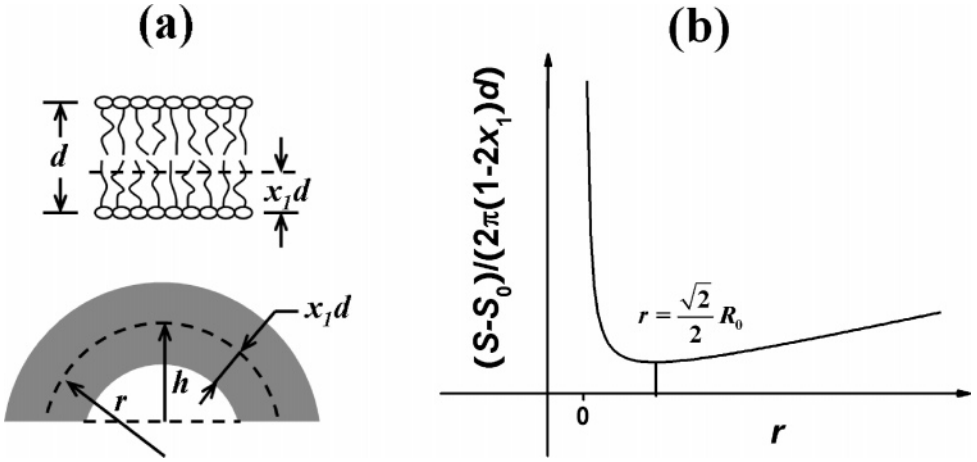

Figure 8. (a) Schematic representation of the domain−water surface energy (area) transition by assuming a plane x_1d distant from the inner surface conserves the area density. (b) Dependence of the domain−water surface area S on the bud curvature ($1/r$). S_0 and $2\pi(1-2x_1d)$ are constant.

normal stress is smaller than the lateral stress in the system.[36] That is, each spot on the membrane repels its surrounding area, so the membrane is not strained. Previous theory predicts that buds only exist when the surface tension is less than 0.01 mN/m^2, corresponding to an almost tensionless membrane.[17] However, it is impossible for DPD simulation to generate such a small surface tension in a controlled way. By adding one lipid in each monolayer, the surface tension would fluctuate from $0.05k_BT/r_c^2$ to $-0.05k_BT/r_c^2$ in the simulation with typical parameters. We have tried our best to generate membranes with a surface tension close to zero. Often it went to slightly negative. We further checked in a single component bilayer, with such slightly negative surface tension it is stable and no buckling occurred (Figures 1a and 4a), so the budding is not induced by pushing the membrane at the boundary. We expect that the finite thickness and curvature elasticity of the lipid bilayer prevent it from buckling. Previous DPD simulations have generated stable bilayer membranes with even more negative surface tensions (up to $-4k_BT/r_c^2$).[22,23] Therefore, we believe the slightly negative value of the surface tension will not cause any serious problem in the study of the membrane evolution.

In this section, we change UCDL and LCDL values, and investigate the effect of surface tension on budding. Results in Table 1 are generated from the simulations where the lipids in the mother membrane have the chain modulus $k_{cA} = 3.0k_BT$, and results in Table 2 have the chain modulus from $k_{cA} = 0.0k_BT$. These data agree with the early results of the surface-tension dependence investigated by a Monge description of the membrane.[17]

The membrane tends to rupture in the region of highly positive surface tension, wherein the membrane patch is tightly strained and each spot on the bilayer has a tendency to pull in the surrounding area. It is analogous to a vesicle with extremely high interior pressure. The fact that the ruptures are always initialized along the domain boundary reveals the relatively larger line tension between the lipid components, A and B, because of their strong repulsive interactions. Indeed, we observe vesicular explosions experimentally when all of the domains coalesce into a single one, but the interfacial energy (line tension) is still high.

In the intermediate tension region, the domain exhibits small curvature or keeps flat, with neither rupture nor budding followed. This state is similar to a spherical vesicle, where domains or caps are floating on the mother membrane, but further deformations are confined by the low area-to-volume ratio.[9−11] Comparing the last two columns of both high and intermediate tension regions in Tables 1 and 2, we find that enlarging the contrast in the bending moduli of the coexisting phase has an equivalent effect to increasing the line tension. In Table 1, as the chain modulus of the domain is raised, the tendency to rupture is remarkably hindered. Likewise, the domain is prone to curve when the bending moduli of the two phases get closer in Table 2. Thus, it can be concluded that the difference in the chain modulus contributes to the structural dissimilarity of the lipid components, or rather the immiscibility of the coexisting phases.

When the surface tension becomes slightly negative but still close to zero, the budding process is induced by the line tension. In this region, the lipids repel strongly against theirs neighbors, resembling the vesicles on which a sufficient excess area is present and produces a pushing effect on surrounding area.[7,8,12] Note that, in the third region in both Table 1 and Table 2, the budding events take place no matter whether the budding phase is more rigid than the mother membrane or not. This is in agreement with the experiments,[10,11] demonstrating that the budding process is determined by the line tension but not by the specific properties, for example, bending moduli, of the two phases.

In addition, two fission pathways are observed at the late stage of budding, as reported previously in simulations[21] of a self-assembled vesicle. One includes the rupture of the neck and the subsequent resealing of the two separated membranes (Figure 12a). In the second pathway, the membrane remains impermeable to the water and undergoes hemifission intermediate, during which the interior monolayer self-fuses while the exterior one maintains integral (Figure 12b). This is a validation

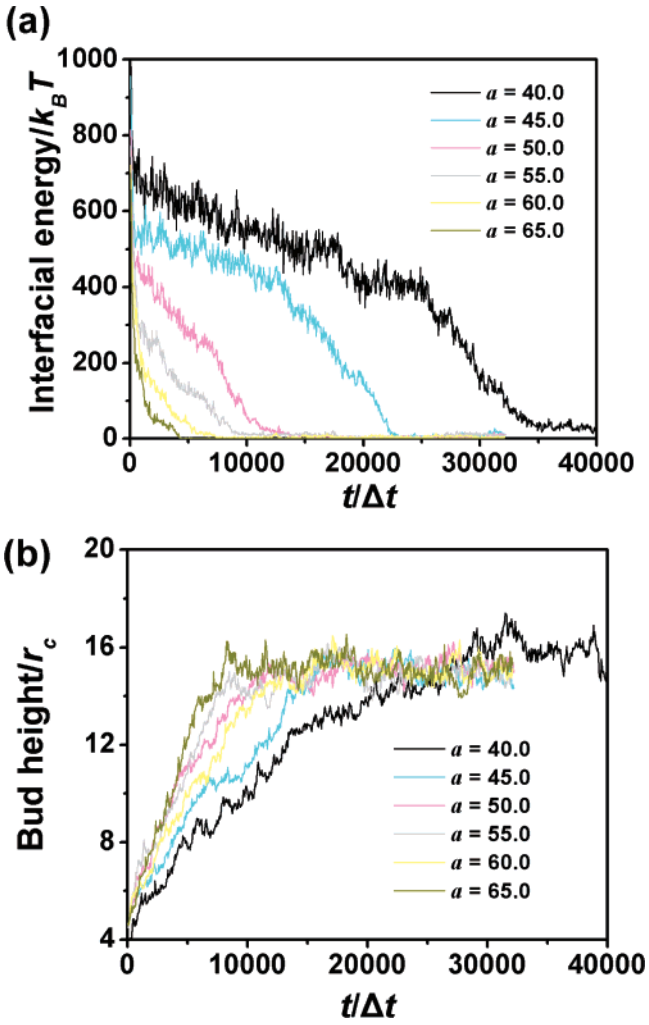

Figure 9. Evolution of bud morphologies in the membranes with different line tensions ($k_{cA} = k_{cB} = 3.0k_BT$). (a) Evolution of the interfacial energy, which is proportional to the interfacial length between the two lipid components A and B. (b) Evolution of bud height, indicating that the buds reach the tallest configurations at the transition point of their corresponding interfacial energy curves in (a).

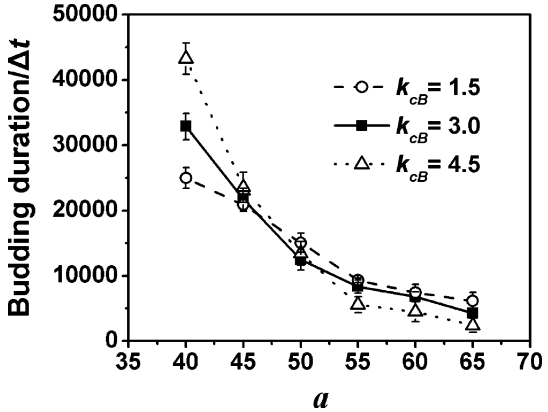

Figure 10. Dependence of budding duration on line tension and bending modulus. The bending modulus of the membrane is characterized by the chain modulus. A larger chain modulus indicates a harder membrane.

that the fission mechanism is not altered by the open membrane morphology and the boundary conditions in *N*-varied DPD.

We compare the budding durations, in Figure 13, of two series of systems imposed with UCDL/LCDL = $2.13r_c^{-2}/0.50r_c^{-2}$ ($\sigma = -0.23k_BT/r_c^2$) and $1.75r_c^{-2}/0.63r_c^{-2}$ ($\sigma = -0.16k_BT/r_c^2$),

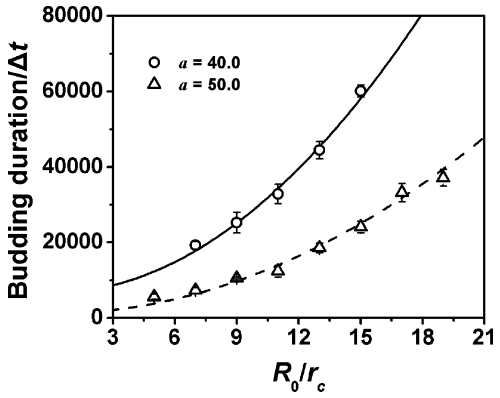

Figure 11. Dependence of budding duration on domain size. The solid line and the dashed line are quadratic fittings to the simulated data according to eq 17.

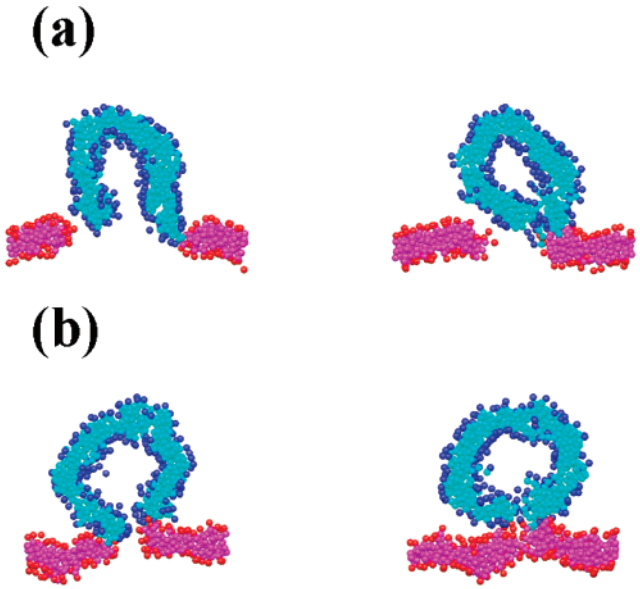

Figure 12. Fission pathways: (a) high line tension leads to cleavage, (b) low line tension leads to hemifission intermediate.

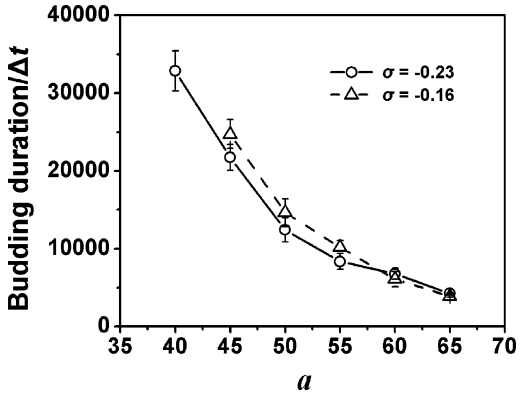

Figure 13. Dependence of budding duration on line tension with different surface tensions.

respectively. The former provides more excess areas than the latter and consequently facilitates the out-of-membrane deformation. However, the effect of surface tension is not significant in the low and high line tension regimes. The duration times both decrease with the increase of the line tension.

D. Tubular Bud Intermediate. The tubular bud (Figure 4c,c′) in our preceding simulations was also experimentally observed on tubular vesicles with diminished encapsulated

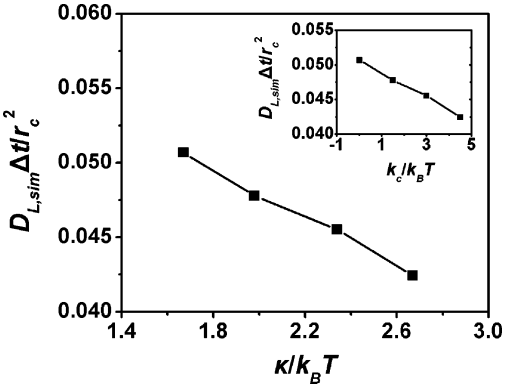

Figure 14. Dependence of lateral diffusion coefficients of lipids on bending modulus κ. The inset shows the dependence of the lateral diffusion coefficients of lipids on the chain modulus k_c. The sizes of error bars are smaller than the squares.

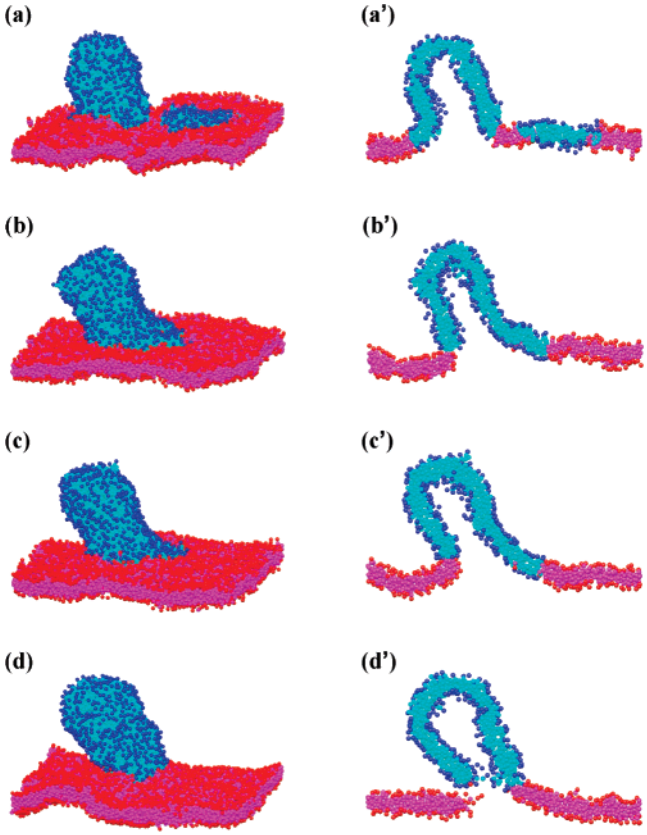

Figure 15. Snapshots of bud-domain coalescence with t = (a) $0\Delta t$, (b) $3000\Delta t$, (c) $4000\Delta t$, and (d) $6000\Delta t$ and (a′)−(d′) their corresponding sliced images .

volume constraint and remained stable throughout the observation period.[12] The morphology may be ascribed to the membrane thickness effect, which acts with a considerable role in DPD and the real multi-lamellar vesicles. However, no stable tubular buds exist in the simulations. We observe either complete vesiculations, wherein the subsequent neck constriction and severing reduce the interface energy between the two lipid components by more than the gain in bending and surface energies, or no budding, in which the line tension is not sufficient to induce the large shape transformation. Thus, we conclude that the experimentally observed tubular bud is actually an intermediate but stands beyond the experimental scale.

The lateral diffusion constants $D_{L,sim}$ of simulated lipids in the single-component membrane with different bending moduli

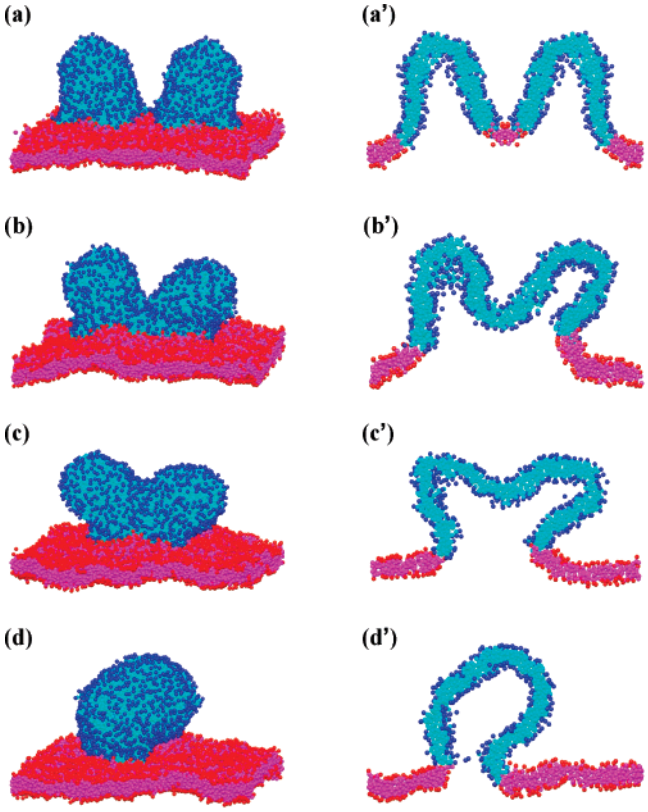

Figure 16. Snapshots of bud−bud coalescence with t = (a) $0\Delta t$, (b) $4500\Delta t$, (c) $6500\Delta t$, and (d) $12\ 500\Delta t$ and (a′)−(d′) their corresponding sliced images.

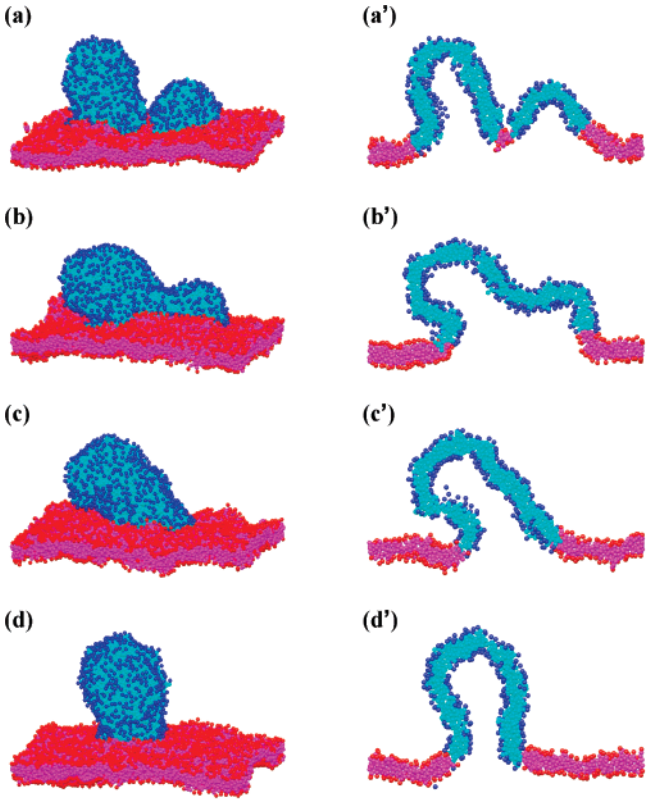

Figure 17. Snapshots of bud-cap coalescence with t = (a) $0\Delta t$, (b) $3500\Delta t$, (c) $7500\Delta t$, and (d) $11500\Delta t$ and (a′)−(d′) their corresponding sliced images.

κ are presented in Figure 14. The inset shows the dependence of $D_{L,sim}$ on chain modulus k_c. Assuming $D_{w,sim}/D_w = D_{L,sim}/$

D_L, where the subscript w denotes water and sim indicates simulation, we map the lateral diffusion constant of lipids to the experimental scale D_L, using the values $D_w = 0.307r_c^2/\Delta t$ simulated on a pure water system, $D_w = 2.57 \times 10^{-5}$ cm^2/s,[39] and $D_{L,sim} = 0.045r_c^2/\Delta t$ estimated from Figure 14. D_L then equals 3.77×10^{-6} cm^2/s. If we take the relation $t/t_{lip} = (R^2/D_L)/(R_{lip}^2/D_{lip})$, which is equivalent to eq 17, and the estimations for the simulated domain size $R \approx 10r_c \approx 10$ nm, the experimental domain sizes $R_{lip} \approx 5$ μm, the lateral diffusion constant for real lipids[40,41] $D_{lip} \approx 8 \times 10^{-8}$ cm^2/s, and $\Delta t = 0.05[m_0r_c^2/(k_BT)]^{1/2} \approx 0.25$ ps (assuming $r_c \sim 10^{-9}$ m and room temperature), the mapped time t_{lip} is around 0.1−1 s for the budding process shown in Figure 5, a bit lower compared with the experimental result (~10 s).[12]

Three typical growth modes in the budding process have been reported in experimental studies.[12] The morphological changes of these growth modes are conveniently reproduced by *N*-varied DPD (Figures 15−17). The initial states are constructed by joining the well-formed buds, caps, or domains together and then evolved with UCDL = $2.13r_c^{-2}$, LCDL = $0.50r_c^{-2}$, and $k_{cA} = k_{cB} = 3.0k_BT$. Figure 15 exhibits the growth of a bud by coalescence with a flat domain. The mergence makes the bud lean toward the direction opposing the domain and grow even longer. The fusion of two tubular buds is shown in Figure 16, wherein the bud tops bend oppositely to avoid the formation of high curvature at the saddle region. In the coalescence of a bud and a cap (Figure 17), the bud leans when the cap merges into the root and restores to the upright configuration afterward.

All of the three modes end with the figure of a longer bud and show an effect to elongate the existence of tubular buds. This inspires us with a second possible fact that contributes to the long life span of the experimental buds besides the large-size effect. That is, individual lipid molecules and small domains merge into the bud continuously from all directions around the root. So, no leaning takes place under the uniformly all-sided collisions, but the neck constriction is effectively delayed by the incessant coalescences.

IV. Summary and Outlook

In summary, we simulate the budding and fission dynamics of individual domains in the flat membrane patches by altering the boundary conditions of normal DPD and making the bead number *N* variable. The modification provides adequate excess areas indispensable for the budding process. Advantageously, the flexibility in controlling the boundary conditions and the morphological simplicity intrinsic of the open, flat bilayer make the *N*-varied DPD especially suitable to explore the effects of elastic properties on budding dynamics and, at the same time, preserve the molecular details. Five stages of budding dynamics are classified according to the bud configurations of the individual domain. Especially, there exists a stage of a tubular bud in our simulation, in which the effect of the membrane thickness cannot be neglected. Both the energy and the morphology evolutions obtained indicate a transition in budding dynamics when a tubular bud forms, including the rise of the domain-water surface energy and the acceleration of constriction of the interface between the two lipid components. The former is out of the dramatic increase in the domain−water surface area after the formation of a tubular bud, and the latter is successfully explained by introducing the hydrodynamic drag force, which is not involved in conventional equilibrium theories, into the dynamic analysis.

In the low line tension regime, extremely high and extremely low bending moduli are unfavorable conditions for bud formation. In contrast, in the regime with high line tension, the budding process is not significantly affected by the bending modulus. Afterward, the controlling role of the surface tension that mainly originates from the area constraints is noted after comparison among the systems imposed with different boundary conditions. Budding is only induced in the prerequisite of sufficient excess area and released surface tension. Finally, we map the simulated results to the experimental scale and conclude that the tubular bud is an intermediate in both simulations and experiments.

However, the lipid architecture adopted here is closer to small surfactants than actual lipids. Simulations of molecules with longer hydrophobic tails or multiple tails can be conducted to study the molecular structural effects and the membrane thickness effects. Further, the domains are initialized unnaturally in our work, which might introduce unexpected artifacts. Thus, we suggest a larger scale simulation, in which a quench from high temperature can be mimicked and the scattered lipids self-aggregate into a circular domain. These works are currently underway.

Acknowledgment. We would like to thank Li Li, Kunkun Guo, and Mingzhu Sun for helpful discussions. We are grateful for the financial support from the National Natural Science Foundation of China (Grant Nos. 20625413, 20574015, and 20490220) and the Ministry of Education of China (FANEDD 200225). The simulations were run on IA64Beowulf clusters in the Supercomputing Center of Fudan University.

References and Notes

(1) Lipowsky, R.; Sackmann, E. *Handbook of biological physics;* Elsevier: Amsterdam, The Netherlands, 1995; Vol. 1.
(2) Sprong, H.; Van der Sluijs, P.; Van Meer, G. *Mol. Cell. Biol.* **2001**, *2*, 504.
(3) Van Meer, G.; Sprong, H. *Curr. Opin. Cell Biol.* **2004**, *16*, 373.
(4) Lipowsky, R. *J. Phys. II* **1992**, *2*, 1825.
(5) Jülicher, F.; Lipowsky, R. *Phys. Rev. Lett.* **1993**, *70*, 2964.
(6) Kohyama, T.; Kroll, D. M.; Gompper, G. *Phys. Rev. E: Stat. Phys., Plasmas, Fluids, Relat. Interdiscip. Top.* **2003**, *68*, 61905.
(7) Laradji, M.; Kumar, P. B. S. *Phys. Rev. Lett.* **2004**, *93*, 198105.
(8) Laradji, M.; Kumar, P. B. S. *J. Chem. Phys.* **2005**, *123*, 224902.
(9) Veatch, S. L.; Keller, S. L. *Phys. Rev. Lett.* **2002**, *89*, 268101.
(10) Baumgart, T.; Hess, S. T.; Webb, W. W. *Nature* **2003**, *425*, 821.
(11) Bacia, K.; Schwille, P.; Kurzchalia, T. *Proc. Natl. Acad. Sci. U.S.A.* **2005**, *102*, 3272.
(12) Li, L.; Liang, X. Y.; Lin, M. Y.; Qiu, F.; Yang, Y. L. *J. Am. Chem. Soc.* **2005**, *127*, 17996.
(13) Helfrich, W. *Z. Naturforsch.* **1973**, *28c*, 693.
(14) Ou-Yang, Z. C.; Helfrich, W. *Phys. Rev. Lett.* **1987**, *59*, 2486.
(15) Andelman, D.; Kawakatsu, T.; Kawasaki, K. *Europhys. Lett.* **1992**, *19*, 57.
(16) Kumar, P. B. S.; Gompper, G.; Lipowsky, R. *Phys. Rev. E: Stat. Phys., Plasmas, Fluids, Relat. Interdiscip. Top.* **1999**, *60*, 4610.
(17) Harden, J. L.; MacKintosh, F. C.; Olmsted, P. D. *Phys. Rev. E: Stat. Phys., Plasmas, Fluids, Relat. Interdiscip. Top.* **2005**, *72*, 011903.
(18) Kumar, P. B. S.; Rao, M. P*hys. Rev. Lett.* **1998**, *80*, 2489.
(19) Kumar, P. B. S.; Gompper, G.; Lipowsky, R. *Phys. Rev. Lett.* **2001**, *86*, 3911.
(20) Yamamoto, S.; Maruyama, Y.; Hyodo, S. *J. Chem. Phys.* **2002**, *116*, 5842.
(21) Yamamoto, S.; Hyodo, S. *J. Chem. Phys.* **2003**, *118*, 7937.
(22) Shillcock, J. C.; Lipowsky, R. *J. Chem. Phys.* **2002**, *117*, 5048.
(23) Illya, G.; Lipowsky, R.; Shillcock, J. C. *J. Chem. Phys.* **2005**, *122*, 244901.
(24) Rekvig, L.; Hafskjold, B. *J. Chem. Phys.* **2004**, *120*, 4897.
(25) Rekvig. L.; Hafskjold, B.; Smit, B. *Phys. Rev. Lett.* **2004**, *92*, 116101.
(26) Jakobsen, A. F.; Mourisen, O. G. *J. Chem. Phys.* **2005**, *122*, 204901.
(27) Yamamoto, S.; Hyodo, S. *J. Chem. Phys.* **2005**, *122*, 204907.
(28) Li, D.; Liu, X. Y. *J. Chem. Phys.* **2005**, *122*, 174909.
(29) Hoogerbrugge, P. J.; Koelman, J. M. V. A. *Europhys. Lett.* **1992**, *19*, 155.

(30) Español, P.; Warren, P. *Europhys. Lett.* **1995**, *30*, 191.
(31) Groot, R.; Warren, P. *J. Chem. Phys.* **1997**, *107*, 4423.
(32) Pagonabarraga, I.; Hagen, M.; Frenkel, D. *Europhys. Lett.* **1998**, *42*, 377.
(33) Vattulainen, I.; Karttunen, M.; Besold, G.; Polson, J. M. *J. Chem. Phys.* **2002**, *116*, 3967.
(34) Kirkwood, J. G.; Buff, F. P. *J. Chem. Phys.* **1949**, *17*, 338.
(35) Leach, A. R. *Molecular Modeling: Principles and Applications*, 2nd ed.; Prentice Hall: New York, 2001.
(36) Goetz, R.; Lipowsky, R. *J. Chem. Phys.* **1998**, *108*, 7397.
(37) Goetz, R.; Gompper, G.; Lipowsky, R. *Phys. Rev. Lett.* **1999**, *82*, 221.
(38) Berg, H. C. *Random Walks in Biology*; Princeton University Press: Princeton, 1993.
(39) Wang, J. H. *J. Phys. Chem.* **1965**, *69*, 4412.
(40) Orädd, G.; Lindblom, G.; Westerman, P. W. *Biophys. J.* **2002**, *83*, 2702.
(41) Filippov, A.; Orädd, G.; Lindblom, G. *Biophys. J.* **2004**, *86*, 891.